EXPERIMENTAL AND NUMERICAL ANALYSIS OF STEEL FIBER REINFORCED CONCRETE SLABS

Barros, J. A. O.[1]
Figueiras, J. A.[2]
[1]School of Engineering, University of Minho
Azurém, 4800 Guimarães, Portugal, Tel: 351-53-510210
[2]Civil Eng. Dept. Faculty of Engineering, University of Porto
Ruas dos Bragas, 4099 Porto, Portugal, Fax: 351-2-2003640, Tel: 351-2-2041948

Abstract: Steel fiber reinforced concrete (*SFRC*) has proven to be an attractive material for a wide range of applications in civil construction industry. The excellent performance exhibited by this composite is essentially due to its high energy absorption capacity.
This paper describes the tests performed and the numerical model developed to simulate the behavior of *SFRC* structures. The influence of steel fibers on the behavior of concrete structures with fracture mode *I* was assessed by performing bending tests on slab strips reinforced with different percentage of fibers and including a conventional wire mesh reinforcement, as well. Fiber concentration ranged from 0 to 2.5 percent by weight of concrete. The hooked-ends steel fibers, with the trademark *Dramix ZX60/.80*, were the fibers considered in this study.
A significant increase in the load carrying capacity of the slabs and a decrease in the crack spacing were observed with the increasing of fiber content.
The constitutive model developed is based on the strain decomposition concept for the cracked cement based materials. This concept is adjusted to simulate the fiber reinforcement contribution. The model performance was assessed by the experimental results obtained.

1 - INTRODUCTION

The inclusion of fibers in cement based materials improves the performance of these composites (*ACI 1982*). Amongst the properties most benefited by fiber reinforcement, it can be distinguished the energy absorption capacity, the fatigue and impact strength. The cracking behavior is also improved by the presence of fibers crossing the micro-cracks. Due to the mechanical and physical enhancements, a wide range of fiber reinforced concrete products has been used in civil construction industry (*ACI 1982,RILEM 1986,Balaguru 1992*).

In now-a-days, good fast construction in big cities is a mandatory requisite to achieve the economical and functional performances. Prefabrication of structural elements is well adjusted to this objectives (*Cederqvist 1987*). Prefabricated simply supported slab strips reinforced with wire mesh have being used in the construction of pavements of silo-autos, shopping-centers, etc.. The flexural strength, toughness and ductility of these slabs can be increased by fiber addition to the mix (*Clarke 1987*).

In order to evaluate these improvements, an experimental and numerical research program was developed to study the behavior of steel fiber reinforced concrete (*SFRC*) slab strips. In this paper the main experimental results are presented, the numerical model developed is briefly described and its ability to predict the behavior of these structures is illustrated.

2 - COMPOSITION, CASTING AND PROPERTIES

Mixture proportions - Table 1 presents the mixture proportions used in the experimental program.

Component	(kg/m^3)
Cement	450
Aggregates (a) Fine (0-3 mm)	819
Aggregates (a) Coarse (0-15 mm)	910
Water	157.5
Additive (*Rheobuild 561.*)	4.5
DRAMIX steel fibers *ZX60/.80*	0, 30, 45, 60
Characteristics	
w/c	0.35
c/a	0.26
Additive (% in weight by cement)	1
W_f (% of fibers in weight of mixture)	0, 1.25, 1.85, 2.5

Table 1 - Mixture proportions.

Mixing procedure - A conventional equipment was used in the mixing procedure. The aggregates were washed and dried before mixing. To prevent the segregation or balling of the fibers during mixing, and to get the desired workability (*ACI 1984*), different mixing sequences were attempted. The following mixing sequence was found to work efficiently for the mixtures designed: water, cement, coarse aggregates, sand and fibers. The mixing time depends on the mixture characteristics, as well on the concrete content-mixer capacity ratio (*Balaguru 1992*). This ratio should decrease with increasing the fiber content and fiber aspect-ratio (length-diameter ratio). The mixing time should be the necessary to warrant a uniform dispersion of fibers throughout the mixture. For instance, to mix approximately 100 *l* of *SFRC* (≈ 50% of the mixer capacity) it was spent about 3 minutes.

Casting procedure - The slab strips, with 1800x50x75 mm, were casted in a timber mould, faced with a zinc plate. An external vibration of the forms was applied.

Curing procedure - Until demoulding (at approximately 7 days) the slab strips and the corresponding cylinder and prismatic specimens were kept with wet cloths, remaining in the natural environment of the laboratory (65% RH and 20ºC) until time of test.

Properties measured in specimens - For each slab strip, at least two prismatic specimens of dimensions 600x150x150 mm and two cylinders of 150 mm diameter and 300 mm height were tested, in order to assess the bending and compression behavior, respectively. The average compression strength, f_{cm}, and the average net bending stress at maximum load, f_{fnet}, (*Barros 1995b*) are presented in Table 2 for each slab strip specimens.

Content of fibers (kg/m^3)	f_{cm} (MPa)		f_{fnet} (MPa)
	At test age [days]	At 28 days	[days]
0	65.8 [217]	56.0	6.41 [298]
30	61.5 [204]	52.5	6.38 [284]
45	59.9 [176]	51.6	7.53 [223]
60	59.1 [124]	51.8	8.64 [208]

Table 2 - Average compression strength and net bending stress of slab strip specimens.

3 - TESTS OF SLAB STRIPS

3.1 - Equipment and slab reinforcement

Figure 1 shows a slab strip installed in the testing rig and a schematic representation of the measuring devices and load arrangement.

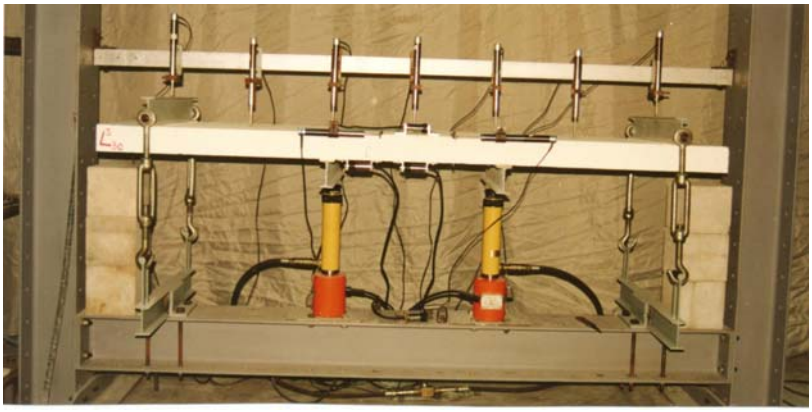

(a)

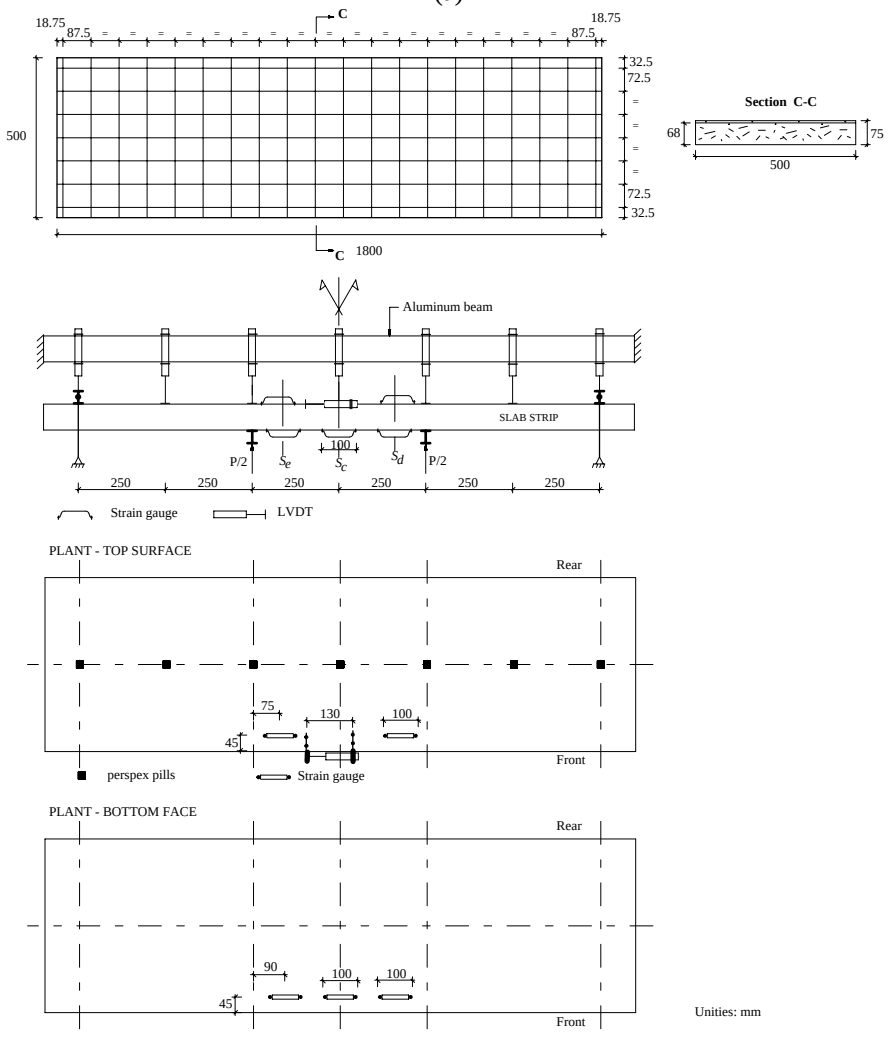

(b)

Figure 1 - Setup of a slab strip test (a), slab strip geometry, support and load arrangement and details of instrumentation (b).

The load was obtained from two load cells of 50 kN maximum capacity, while the displacements were measured with *LVDTs* (Linear Variable Differential Transducers) of 30 mm of measuring range, attached to a bar fixed to the external supporting structure. Strain gauges with 8 mm of measuring length were applied to the top and bottom surfaces between point loads. The signals of the *LVDTs* and load cells were amplified, sent to a personal computer, converted from analog to digital and saved for posterior post-processing. Two slab strips reinforced with 0, 30, 45 and 60 kg/m^3 of steel fibers and including a wire mesh were tested. The wire mesh was made of wires of 2.7 mm in diameter with a transverse and longitudinal spacing of 175 mm and 145 mm, respectively. The reinforcement of each slab strip consists of two crossover wire mesh, leading to a transverse and longitudinal spacing of 87.5 mm and 72.5 mm, respectively, and an area of longitudinal reinforcement of 40 mm^2 in the slab width (see Figure 1). This reinforcement is placed in the slab strip tensile face with a concrete cover of 3 mm. The yield stress and the tensile strength, determined for the wire mesh steel, was 560 MPa and 800 MPa, respectively. According to *CEB-FIP* model code 1990 *(CEB-FIP 1990*) and taking into account the average compression strength recorded in specimens' tests, it will be necessary a 40.6 mm^2 of longitudinal reinforcement area, in order to control the cracking (*Barros 1995b*). Therefore, this area is a little bit higher the one employed in slab strips, so that, it is a proper amount of reinforcement to evidence the benefits of fiber reinforcement.

3.2 - Results

In Figure 2 it is shown the typical crack patterns developed in the slab strips tested.

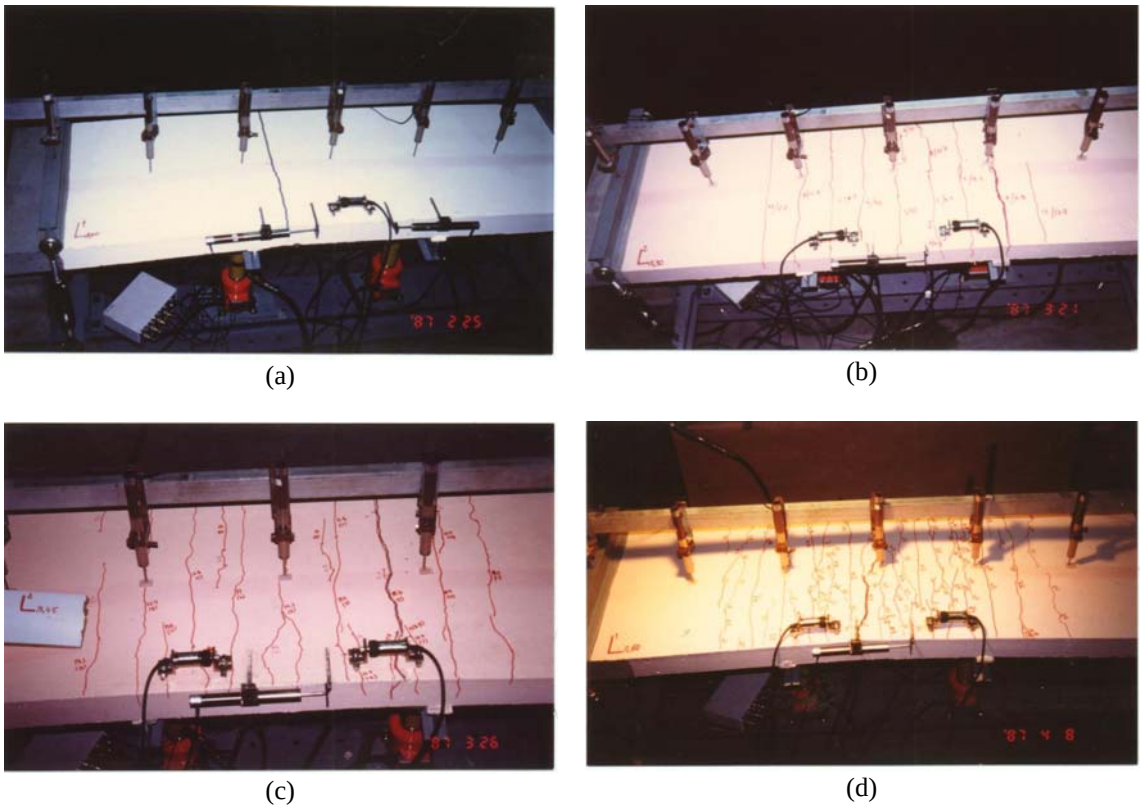

(a) (b)

(c) (d)

Figure 2 - Typical crack patterns of slab strips reinforced with wire mesh and 0 (a), 30 (b), 45 (c) and 60 kg/m^3 (d) of *ZX60/.80* steel fibers.

It is verified that the average crack spacing decrease with the fiber content increment. For wire mesh slab strips reinforced with 30, 45 and 60 kg/m^3 of fibers, it was measured an average crack spacing of 100, 80 and 40 mm between point loads (central span), while for the slab strip reinforced with wire mesh only, an unique crack was developed. The collapse of the slab strips always occurred by the failure of the longitudinal wire mesh, near the section where the longitudinal and transverse wires were welded. This fact reveal that the welded process has weaken the wire steel strength. In Figure 3 it is shown the relationship between the load and the displacement at mid span. The energy absorption capacity and the failure load increase significantly with the increment of fiber content. The value of the failure load of each slab strip tested is specified in Table 3, as well the percentage of load increment with fiber content.

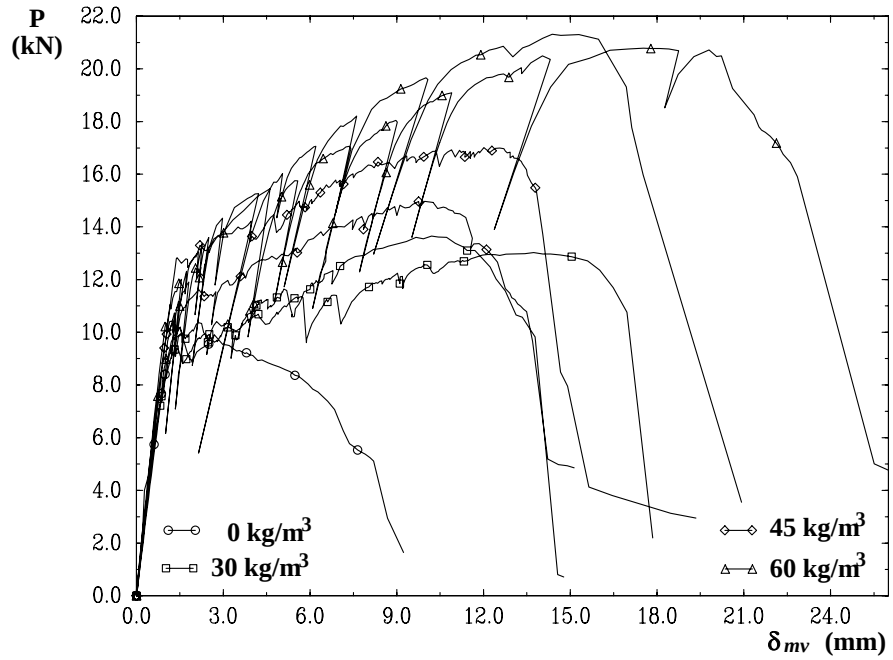

Figure 3 - Relationship between load and displacement at mid span, for the slab strips reinforced with wire mesh and different percentage of steel fibers *ZX60/.80*.

Content of fibers (kg/m^3)	P_{max} (kN)	$\overline{P}_{max}$ (kN)	$\frac{\overline{P}_{max,V_f \neq 0} - \overline{P}_{max,W_f = 0}}{\overline{P}_{max,W_f = 0}} 100$
0	10.2	10.2	-
30	13.7 13.0	13.35	31
45	17.0 15.0	16.0	57
60	20.8 21.3	21.05	106

Table 3 - Maximal (P_{max}) and average ($\overline{P}_{max}$) failure load, and percentage increase on the failure load.

4 - NUMERICAL MODEL

A smeared crack model was developed for nonlinear analysis of concrete laminate structures reinforced with fibers and even with conventional reinforcement. Among the available smeared crack models, it was selected the one based in the strain decomposition concept for the cracked concrete (*de Borst 1985,Barros 1995b*). According to this concept, a cracked concrete is regarded as cracks with concrete between cracks, as it is schematically represented in Figure 4.

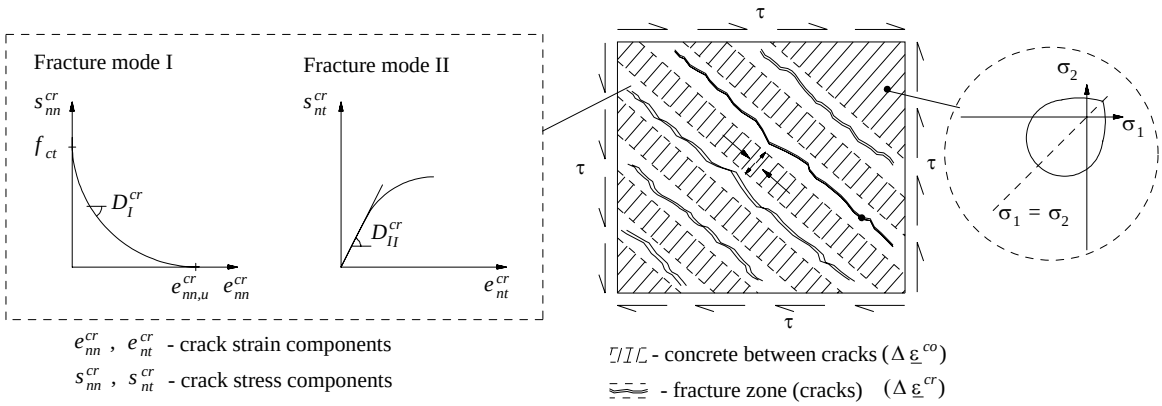

Figure 4 - Schematic representation of the strain decomposition concept for cracked concrete.

In this model the total strain increment of cracked concrete, $\Delta\underline{\varepsilon}$, is the addition of the strain increment in the fracture zone, $\Delta\underline{\varepsilon}^{cr}$ (the width of the finite element over which the micro-cracks are smeared out) with the strain increment in concrete between cracks, $\Delta\underline{\varepsilon}^{co}$.The fracture mode I (D_I^{cr}) and mode II (D_{II}^{cr}) are simulated in the crack constitutive law (*Rots 1988*). As this law is explicitly included in the formulation, this model allows the simulation of fiber reinforcement benefits in a direct way, namely the increase in the fracture energy and cracked concrete shear rigidity. Due to space limitation requirements, only the aspects related to this constitutive law will be focused. The details of the numerical model developed are described in reference: *Barros 1995b*.

The D_I^{cr} is characterized by the following fracture parameters (*Barros 1995b*): tensile strength, f_{ct}; fracture energy, G_f; shape of the softening law; crack band width, l_b. For low content of fibers, the tensile strength is only marginally increased (*Balaguru 1992,Casanova 1996*). On the contrary, even for low content of fibers, the fracture energy is significantly increased (*Barros 1995a*). Expressions determined from experimental results were proposed to evaluate the fracture energy (*Barros 1995b*). Numerical simulation of experimental tests has revealed that trilinear softening law (Figure 5a) is adjusted for hooked-ends steel fibers reinforced concrete (*Barros 1995a*) but the simplified bilinear diagram shown in Figure 5b is also adequate (*Barros 1995b*).

The residual strain at crack closing is higher in fibrous concrete than in plain concrete. To model this behavior it is proposed the following law (see Figure 5a):

$$e_{nn,l}^{cr} = \eta\, e_{nn,m}^{cr} \tag{1}$$

where $e_{nn,m}^{cr}$ is the maximal attained crack strain normal to the crack, and

$$\eta = \left[1 - \exp\left(-1000\, e_{nn,m}^{cr}\right)\right]\left[1 - \exp\left(-2\ l_f\ / d_f\ V_f\right)\right] \qquad (2)$$

with l_f, d_f e V_f being the length, diameter and volume percentage of fibers.

The D_{II}^{cr} is obtained from the following expression (*Rots 1998*):

$$D_{II}^{cr} = \frac{\beta}{1-\beta} G_c . \qquad (3)$$

where G_c is the transverse modulus of elasticity and β is the shear retention factor, determined from

$$\beta = \left[1 - \frac{e_{nn}^{cr}}{e_{nn,u}^{cr}}\right]^p \qquad c/p = 1{,}2 \text{ or } 3 \qquad (4)$$

for plain concrete, with $e_{nn,u}^{cr}$ beeing the ultimate crack strain (see Figure 4), and

$$\beta = \exp\left(-3\ \frac{d_f}{V_f\ l_f}\ \frac{e_{nn}^{cr}}{e_{nn,u}^{cr}}\right) \qquad (5)$$

for *SFRC*.

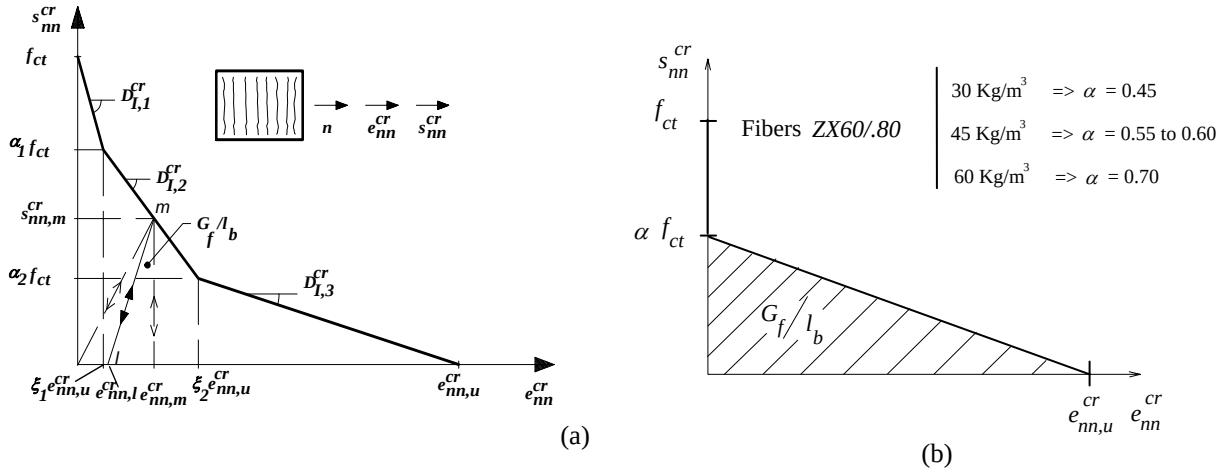

Figure 5 - Trilinear (a) and bilinear (b) softening law for hooked-ends steel fiber reinforced concrete.

5 - MODEL PERFORMANCE

The model performance was assessed by simulating the experimental tests described in Section 3. The section of a slab strip with the position of the wire mesh is shown in Figure 6. Figure 7 illustrates the finite element mesh adopted in the analysis of half slab strip. The load was applied through the displacement control method (*Batoz 1979*). The vertical displacement of node nº 75 (see Figure 7) was selected for control variable. The analysis was performed with a multi-fixed crack model (*Barros 1995b*), where for a sampling point it can be developed, as much, two orthogonal cracks. Table 4 includes the slab strips material properties used in the numerical simulation. The fracture energy values specified in table were obtained with the three-point bending tests on notched beams (*Barros 1995b*). The crack band width is the average crack spacing observed between line loads in the tests performed.

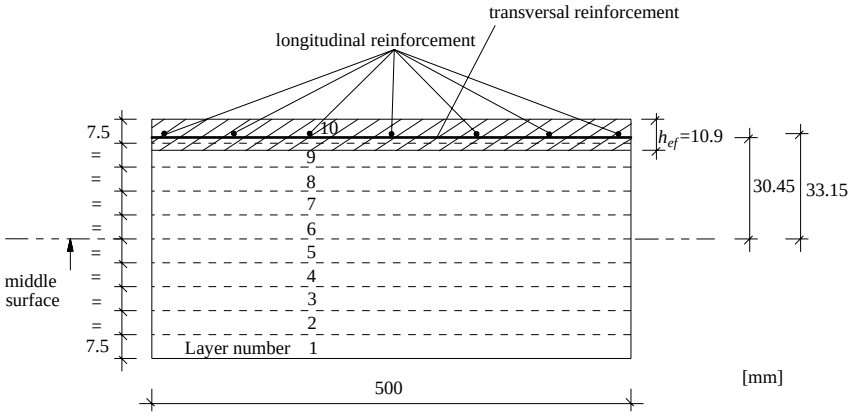

Figure 6 - Transversal section of a *SFRC* slab strip reinforced with wire mesh.

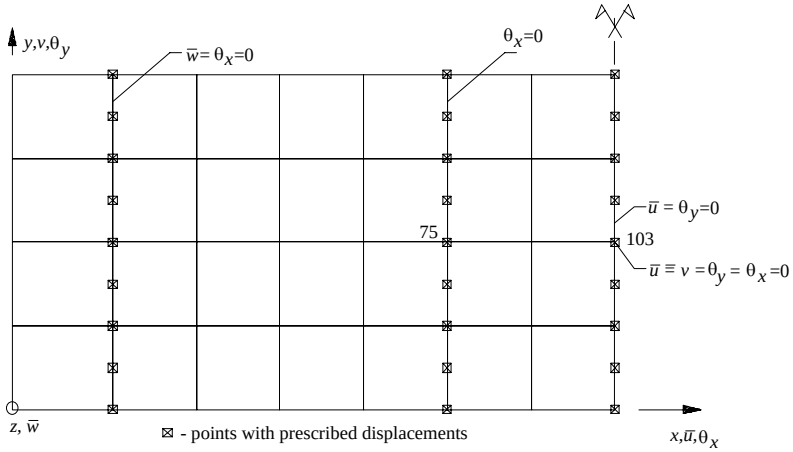

Figure 7 - Finite element mesh used in the discretization of half of a typical slab strip.

Properties	Slab strip reinforced with 30 kg/m^3 of fibers *ZX60/.80*	Slab strip reinforced with 45 kg/m^3 of fibers *ZX60/.80*	Slab strip reinforced with 60 kg/m^3 of fibers *ZX60/.80*
E_c [MPa]	30000	30000	30000
f_c [MPa]	60	60	60
ε_{c1} (x10^{-3}) [-]	3.4	3.5	4.6
f_{ct} [MPa]	4.0	4.0	4.0
Fracture mode I:			
G_f [N/mm]	3.6	9.7	9.7
α ; ζ [-]	0.45 ; 0.005	0.55 ; 0.006	0.70 ; 0.007
l_b [mm]	100	80	40
Fracture mode II: simulated by the expression(5) with l_f / d_f = 75 and V_f =0.38, 0.57, 0.76			

Table 4 - Material properties used in the numerical simulation.

The constitutive law of the steel wire mesh is schematically represented in Figure 8. In slab strip experiments it was verified that, the longitudinal wires crossing the crack had broken when attained the ultimate strain (ε_{sl}), so it follows the descending branch a .

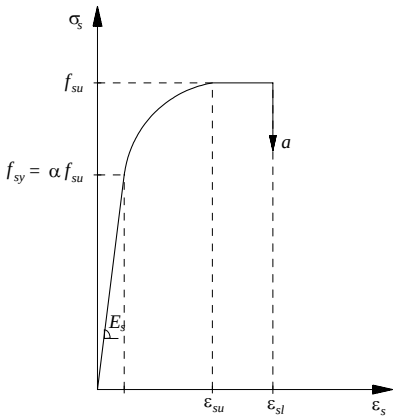

$E_s = 200000\,\text{MPa}$

$f_{su} = 800\,\text{MPa}$

$\alpha = 0.7$

$\varepsilon_{su} = 12e-03$

$\varepsilon_{sl} = 18e-03$

$\rho_l = 0.12,\ \rho_{l,ef} = 0.73,\ \phi_l = 2.7\,\text{mm}$

$\rho_t = 0.094,\ \rho_{t,ef} = 0.58,\ \phi_t = 2.7\,\text{mm}$

Figure 8 - Constitutive law of the wire mesh used.

The experimental and numerical relationship between the load and the vertical displacement at mid-span was shown in Figure 9. Point *P*1 determines the moment when the reinforcement had attained its failure stress at crack. In the numerical analysis, the reinforcement is removed after this point, in order to simulate the rupture of the longitudinal wires occurred in the experiments. This numerical procedure has captured the decrease of load carrying capacity observed experimentally, but the drop was not so prone as it happened in the experiments. This disagreement was increased with the fiber content increment, because after the macro-crack development, it will be performed a reduction in the fracture energy in order to simulate the fracture localization. This procedure was not implemented because it is difficult to evaluate the fracture energy available in the moment when the macro-crack has developed.

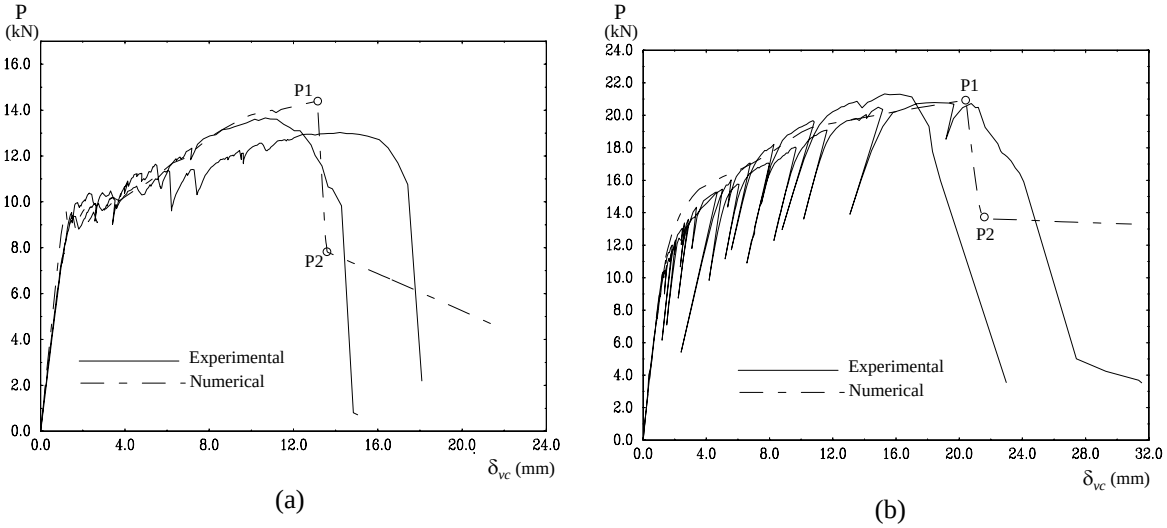

Figure 9 - Relationship between force and vertical displacement at point nº 103 (see Figure 7) for wire mesh concrete slab strips reinforced with 30 (a) and 60 (c) kg/m^3 of *ZX60/.80* steel fibers.

When the point *P*1 was attained, all cracks were in softening branch (the increase in crack strain was followed by a decrease in crack stress). After this point only one macro-crack

has developed, while the remainder cracks enter in the closing process, as it can be shown in Figure 10. This behavior reproduces nicely what was observed in the experiments.

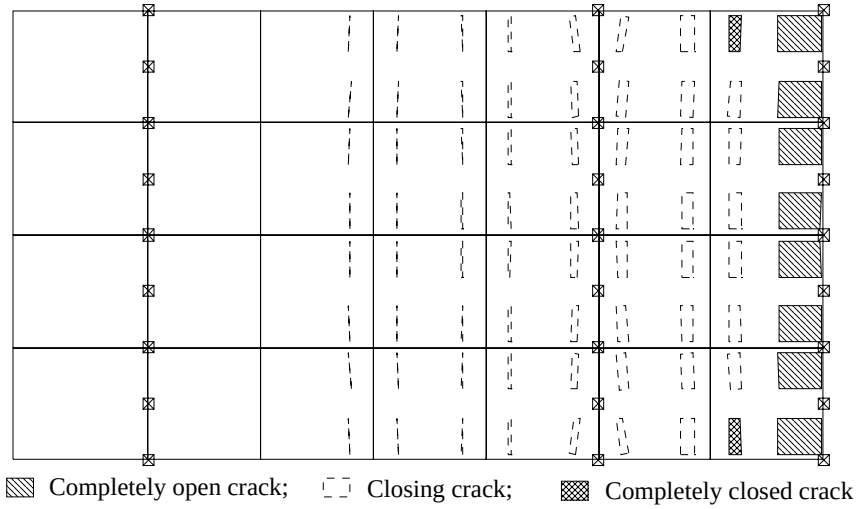

Figure 10 - Typical crack patterns in the top layer at the end loading process (point $P2$ of Figure 9).

6 - CONCLUSIONS

In order to verify the benefits of fiber, slab strips reinforced with different content of hooked-ends steel fibers were tested. The slab strips were also reinforced with conventional wire mesh. For the fiber contents employed (≤ 60 kg/m^3) the cracking load was marginally increased. However, a significant increase in the load carrying capacity and ductility, and a smaller crack spacing with the increment of fiber content was verified. The average failure load of slab strips reinforced with 60 kg/m^3 of fibers was 2.1 times the average failure load of concrete slab strips reinforced with wire mesh only. The average crack spacing was reduced from 100 mm in the slabs reinforced with 30 kg/m^3 to 40 mm in those reinforced with 60 kg/m^3. A brittle failure mode with an unique crack was observed in slab strips reinforced with wire mesh only.

In this sort of steel fiber reinforced concrete (*SFRC*) structures, a maximum crack opening criteria should be mandatory for designing, in order to retrieve the benefits induced by fiber reinforcement. The maximum crack opening should be dependent on the environment aggressiveness, the structure importance and the aesthetic requirements. An adequate numerical model for *SFRC* structures should take into account these factors and should include the fracture energy in the constitutive law that simulates the fracture zone behavior, since it is the property most benefited by fiber reinforcement.

Based on the finite element techniques, a numerical model was developed for nonlinear analysis of *SFRC* structures. Its ability to predict the behavior observed in the experiments with *SFRC* slab strips was highlighted.

7 - ACKNOWLEDGMENTS

The authors wish to thank the PRAXIS XXI/272.1/GEG/33/94 and the JNICT for providing support of the present research program. Support for Bekaert Corporation, Soares da Costa, SEOP, Master Builders Technologies and Socitrel Companies is also gratefully acknowledged.

8 - REFERENCES

1. - ACI Committee 544**,** *State-of-the-Art Report on Fiber Reinforced*, Concrete International: Design & Construction, 22 pages, May 1982.
2. - ACI Committee 544, *Guide For Specifying, Mixing, Placing, and Finishing Steel Fiber Reinforced Concrete*, Fiber Reinforced Concrete International Symposium ACI SP-81, pp. 441-447, 1984.
3. - Balaguru, P.N. and Shah, S.P., *Fiber reinforced cement composites*, McGraw-Hill International Editions, Civil Engineering Series, 530 pages, 1992.
5. - Barros, J.A.O., Figueiras, J.A., *Modelo para estruturas de betão fendilhado reforçado com fibras de aço*, XVI CILAMCE, Brasil, Novembro, 1995a.
6. - Barros, J.A.O, *Comportamento do betão reforçado com fibras, análise experimental e simulação numérica*, PhD Thesis (in Portuguese), Faculty of Engineering, University of Porto, Porto, Portugal, December of 1995b.
7. - Batoz, J.L., Dhatt, G.,*Incremental displacement algorithms for nonlinear problems*, Int. Jour. Num. Meth. Vol. 14, pp. 1262-1267, 1979.
8. - CEB-FIP Model Code, *Design Code*, Bulletin d'information, CEB, Lausanne, Switzerland, 1990.
9. - Cederqvist, H., *Prefabrication of load bearing structures in steel fiber reinforced shotcrete*, Fiber Reinforced Concrete Properties and Applications, SP-105, ACI, pp. 367-374, 1987.
10. - Clarke, R. and Sharma, A., *Flexural behavior of fibro-ferrocrete one-way slabs*, Fiber Reinforced Concrete Properties and Apllications, SP-105, ACI, pp. 493-516, 1987.
11. - De Borst, R.; Nauta, P., *Non-orthogonal cracks in a smeared finite element model*, Eng. Computations., Vol. 2, pp. 35-46, March, 1985.
12. - Casanova, P., *Bétons renforcés de fibres métalliques du matériau à la structure*, Thèse de Doctorat, Laboratoire Central des Ponts et Chaussées, Février 1996.
13. - RILEM Symposium FRC 86, Developments in Fibre Reinforced Cement and Concrete, 1986.
14. - Rots, J.G., *Computational modeling of concrete fracture*, Dissertation, Delft University of Technology, 1988.